ACS APPLIED MATERIALS & INTERFACES

Research Article

www.acsami.org

Hierarchically Structured Ni_3S_2/Carbon Nanotube Composites as High Performance Cathode Materials for Asymmetric Supercapacitors

Chao-Shuan Dai,[†] Pei-Yi Chien,[†] Jeng-Yu Lin,[‡] Shu-Wei Chou,[‡] Wen-Kai Wu,[†] Ping-Hsuan Li,[†] Kuan-Yi Wu,[†] and Tsung-Wu Lin*[,†]

[†]Department of Chemistry, Tunghai University, No. 181, Sec. 3, Taichung Port Rd., Taichung City 40704, Taiwan

[‡]Department of Chemical Engineering, Tatung University, No. 40, Sec. 3, Chungshan North Rd., Taipei City 104, Taiwan

Supporting Information

ABSTRACT: The Ni_3S_2 nanoparticles with the diameters ranging from 10 to 80 nm are grown on the backbone of conductive multiwalled carbon nanotubes (MWCNTs) using a glucose-assisted hydrothermal method. It is found that the Ni_3S_2 nanoparticles deposited on MWCNTs disassemble into smaller components after the composite electrode is activated by the consecutive cyclic voltammetry scan in a 2 M KOH solution. Therefore, the active surface area of the Ni_3S_2 nanoparticles is increased, which further enhances the capacitive performance of the composite electrode. Because the synergistic effect of the Ni_3S_2 nanoparticles and MWCNTs on the capacitive performance of the composite electrode is pronounced, the composite electrode shows a high specific capacitance of 800 F/g and great cycling stability at a current density of 3.2 A/g. To examine the capacitive performance of the composite electrode in a full-cell configuration, an asymmetric supercapacitor device was fabricated by using the composite of Ni_3S_2 and MWCNTs as the cathode and activated carbon as the anode. The fabricated device can be operated reversibly between 0 and 1.6 V, and obtain a high specific capacitance of 55.8 F/g at 1 A/g, which delivers a maximum energy density of 19.8 Wh/kg at a power density of 798 W/kg. Furthermore, the asymmetric supercapacitor shows great stability based on the fact that the device retains 90% of its initial capacitance after a consecutive 5000 cycles of galvanostatic charge−discharge performed at a current density of 4 A/g.

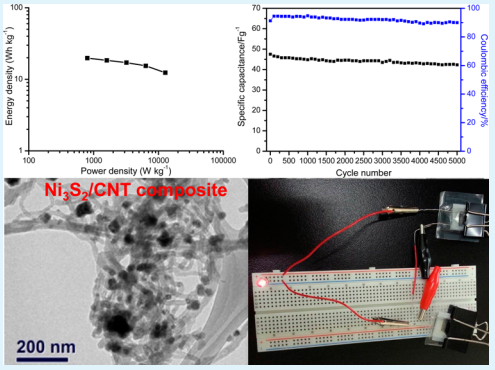

KEYWORDS: *nickel sulfide, carbon nanotube, composite, cathode material, asymmetric supercapacitor*

1. INTRODUCTION

In recent years, supercapacitors have attracted much attention because their unique properties include long cycling lifetime, low maintenance cost, and high power density.[1−3] Furthermore, supercapacitors show great potential applications such as energy-storage systems for portable electronic devices and hybrid electric vehicles.[4] In general, supercapacitors can be classified into two categories based on energy storage mechanisms. One type is the electrical double layer capacitor (EDLC), where the capacitance stems from the pure electrostatic charge accumulated at the electrode/electrolyte interface and the other is the pseudocapacitor, in which the reversible redox reactions take place due to the presence of electro-active species in the electrodes. The pseudocapacitor usually shows a higher value of specific capacitance (C_m) than EDLC due to the presence of the Faradaic process. However, both EDLC and the pseudocapacitor show lower specific energy densities than batteries. Therefore, the development of the supercapacitors with high power and energy densities is still a challenge.

The most well-known materials with pseudocapacitive properties are metal oxide[5−8] and conducting polymers.[9−12] Recently, it has been demonstrated that nickel sulfides (NiS) with various nanostructures including nanoparticles, nanoflakes, and hollow nanospheres display high capacitive performance and great long-term stability, suggesting that NiS is a promising supercapacitor electrode material.[13−15] Furthermore, the combination of NiS and conductive carbon nanomaterials (CNs) such as multiwalled carbon nanotubes (MWCNTs) and reduced graphene oxide (rGO) further enhances the electrochemical properties of these composite electrodes.[16,17] For example, the composite of NiS and rGO exhibits a high C_m value of 1000 F g^{-1} at a current rate of 10 A g^{-1}.[17] The improved capacitive properties of the composites of NiS and CNs may be attributed to the structural advantages. First, the high surface area of CNs enables the electroactive materials to be homogeneously distributed over their surface. Second, the

Received: September 25, 2013
Accepted: November 5, 2013
Published: November 5, 2013

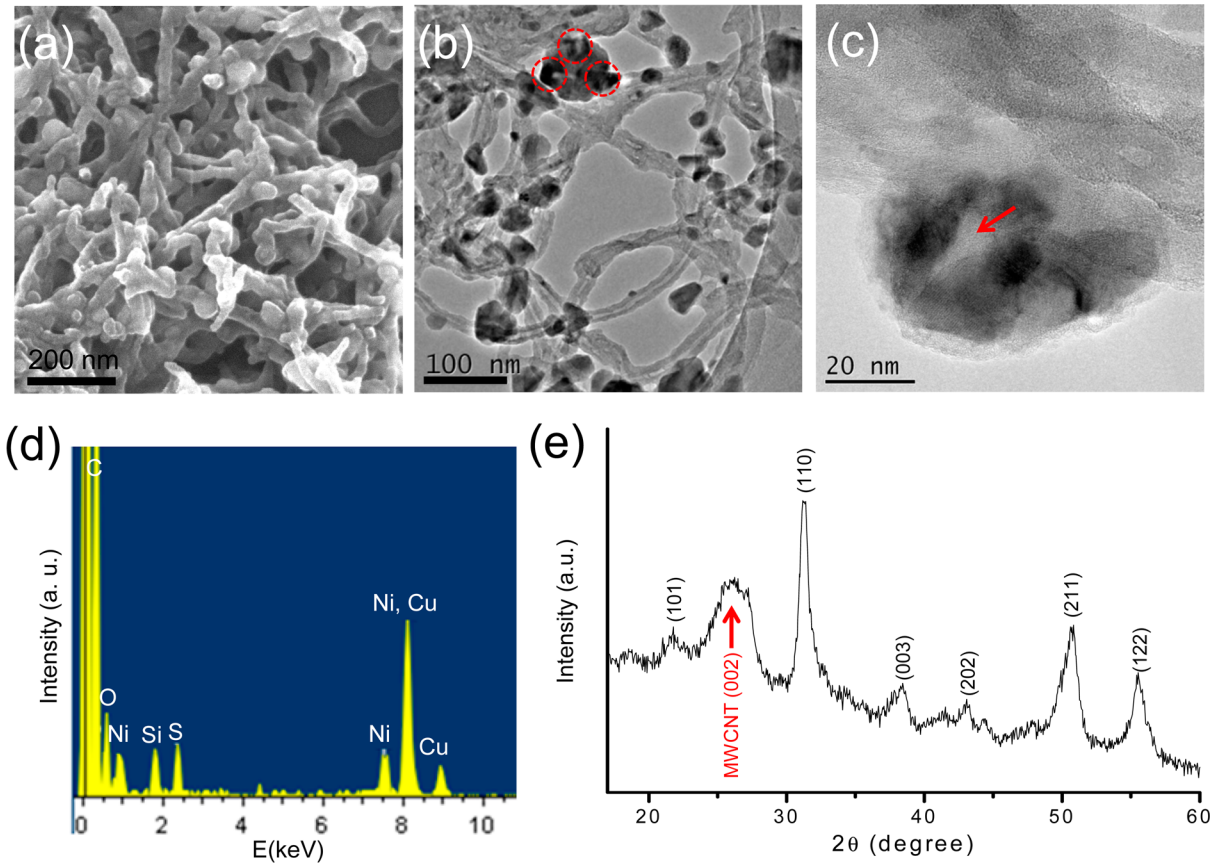

Figure 1. (a and b) SEM and TEM images of Ni_3S_2/MWCNT-NC, respectively. (c) High resolution TEM image, (d) EDS spectrum, and (f) XRD pattern of Ni_3S_2/MWCNT-NC.

high conductivity of CNs allows the electrons to be easily shuttled between a current collector and electroactive materials. Third, the great chemical and mechanical stabilities of CNs improve the cycling performance of supercapacitors. Finally, the open porous network formed by the entanglement of CNs allows the ions to diffuse easily to the surface of the electroactive materials.

In this work, we develop a glucose-assisted hydrothermal method to directly grow Ni_3S_2 nanoparticles on the MWCNT surface and demonstrate that this hierarchical hybrid can serve as the electrode material for supercapacitors. It is found that the use of glucose in hydrothermal reaction is essential to the synthesis of the composite of Ni_3S_2 and MWCNTs (Ni_3S_2/MWCNT-NC). Furthermore, the Ni_3S_2 nanoparticles deposited on MWCNTs disassemble into smaller components after the composite electrode is activated by the consecutive cyclic voltammetry (CV) scan in a 2 M KOH solution, which further increases the active surface area of the Ni_3S_2 nanoparticles on MWCNTs. Due to the synergistic effect of the Ni_3S_2 nanoparticles and the MWCNTs, the Ni_3S_2/MWCNT-NC electrode exhibits a high C_m value and excellent stability in the KOH solution. To evaluate the capacitive performance of the Ni_3S_2/MWCNT-NC electrode in a full-cell configuration, an asymmetric supercapacitor device was fabricated by using Ni_3S_2/MWCNT-NC as the cathode and activated carbon (AC) as the anode. The fabricated device can be operated reversibly between 0 and 1.6 V, and obtain a high specific capacitance of 55.8 F g^{-1} at 1 A g^{-1}, which delivers a maximum energy density of 19.8 Wh/kg at a power density of 798 W/kg. Furthermore, the asymmetric supercapacitor shows a great stability based on the fact that the device retains 90% of its initial capacitance after 5000 cycles of galvanostatic charge−discharge performed at a current density of 4 A/g.

2. EXPERIMENTAL SECTION

2.1. Synthesis of Ni_3S_2/MWCNT-NC. The purification of MWCNTs was achieved by refluxing MWCNTs (0.5 g) in concentrated nitric acid (100 mL) at 120 °C for 12 h. After the reaction, the MWCNT precipitate was filtered off, washed with distilled water, and dried in air. For the synthesis of Ni_3S_2/MWCNT-NC, acid-treated MWCNTs (7.5 mg) and glucose (90 mg) were added to the mixture solution of ethanol (9 mL) and distilled water (1 mL). The mixed solution was sonciated for 20 min to make a homogeneous dispersion and then nickel chloride (195 mg), thiourea (76 mg), and 1 mL of ammonia were added to the MWCNT dispersion. The mixture was then transferred to a stainless-steel autoclave (20 mL capacity). After sealing, the autoclave was heated to 180 °C for 12 h and then cooled to room temperature. Finally, the precipitate was filtered off, washed with distilled water, and dried in air. The weight percentage of Ni_3S_2 loaded on the composite is ca. 80 wt %. In a separate experiment, the Ni_3S_2 powder was synthesized also using the glucose-assisted hydrothermal method. Except for the addition of MWCNTs, the synthetic procedures for Ni_3S_2 powder are the same as those for Ni_3S_2/MWCNT-NC. The diameters of the as-synthesized Ni_3S_2 particles range from 0.5 to 4 μm (Figure S1, Supporting Information).

2.2. Material Characterizations. The surface morphology of Ni_3S_2/MWCNT-NC was characterized using a field emission scanning electron microscope (SEM, JSM-7000F). A field-emission transmission electron microscope (TEM, JEOL JEM-2100F, operated at 200 kV with a point-to-point resolution of 0.19 nm) equipped with an energy dispersive spectrometer (EDS) was used to obtain the

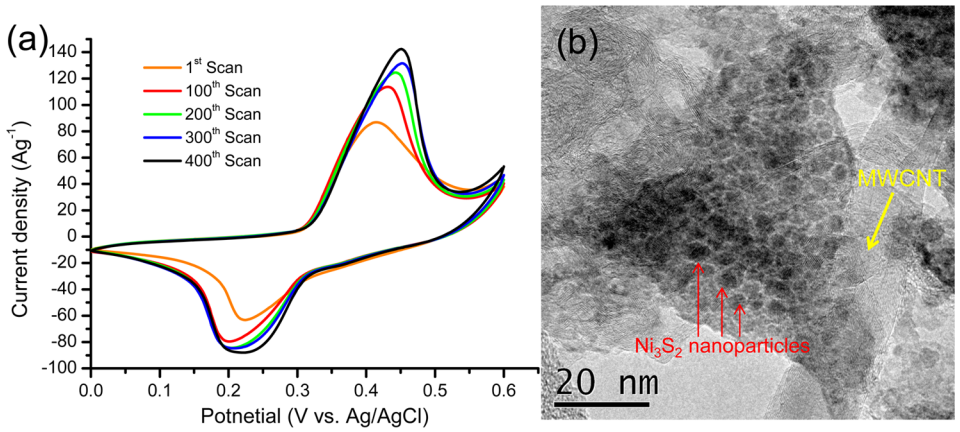

Figure 2. (a) Current density of Ni_3S_2/MWCNT-NC as a function of the number of CV scans. The measurements were performed at a scan rate of 50 mV/s in 2 M KOH. (b) TEM image of Ni_3S_2/MWCNT-NC after the consecutive CV scan. The Ni_3S_2 nanoparticles are indicated by red arrows.

information on the microstructures and the chemical compositions. The X-ray powder diffraction (XRD) pattern of the composite was obtained from Philips X'Pert Pro MPD.

2.3. Electrochemical Measurements. The supercapacitor electrodes were prepared by mixing Ni_3S_2/MWCNT-NC with carbon black and polyvinylidene difluoride (PVDF) at a weight ratio of 8:1:1. After thorough mixing, the slurry was pressed onto Ni foam (10 mm × 10 mm × 1 mm) and then dried at 60 °C in a vacuum for 1 day. The loading of slurry on the Ni foam was approximately 0.6 mg. All electrochemical measurements were performed in a standard three-electrode cell. The Ni_3S_2/MWCNT-NC electrode served as the working electrode, while a Pt wire and an Ag/AgCl (sat. KCl) electrode were used as the counter and a reference electrode, respectively. CV and galvanostatic charge–discharge test measurements were performed using a CHI 635A electrochemical workstation. Electrochemical impedance spectroscopy (EIS) measurements were conducted using a potentiostat (IM6, Zahner) equipped with a frequency analyzer (Thales). An AC voltage with 5 mV amplitude in a frequency range of 0.01 Hz–100 kHz was applied, and the resultant spectra were simulated using Zview software.

2.4. Fabrication of Asymmetric Supercapacitor Devices. To fabricate the asymmetric supercapacitors, AC and Ni_3S_2/MWCNT-NC were used as the anode and the cathode, respectively. The anode was prepared by mixing commercial AC powder with carbon black and polyvinylidene difluoride (PVDF) at a weight ratio of 8:1:1. After thorough mixing, the slurry was pressed onto Ni foam (10 mm × 10 mm × 1 mm) and then dried at 60 °C in a vacuum for 1 day. Two electrodes where the total mass loading of active materials was 1.51 mg were separated by a filter paper. The cell was encapsulated by flexible plastic film with two pieces of platinum wires connected to the edges of the two electrodes. Finally, a 2 M KOH solution was injected into the cell to rinse the filter paper. The electrochemical properties of the asymmetric supercapacitor devices were measured using a CHI 635A electrochemical workstation.

3. RESULTS AND DISCUSSION

The morphology of the sample after hydrothermal reaction was first characterized by SEM. As shown in Figure 1a, the MWCNT surface is decorated with the nanoparticles. Figure 1b shows the typical TEM image of nanoparticle-decorated MWCNTs. It is clear to see that conductive MWCNTs can serve as the backbone where the nanoparticles with the diameters ranging from 10 to 80 nm are deposited. Furthermore, as indicated by the red circles in Figure 1b, the self-assembly of small nanoparticles into irregularly shaped nanoparticles is evidently observed. The selected area electron diffraction (SAED) image of an irregularly shaped nanoparticle shows a ring pattern, suggesting that the nanoparticle is polycrystalline (Figure S2, Supporting Information). It is noteworthy that the use of glucose in the hydrothermal reaction plays a crucial role in the formation of the hybrid structure. As shown in Figure 1c, a layer of amorphous carbon derived from glucose covers both the MWCNT and nanoparticle surface and thus serves as a binder to assist the nanoparticles to grow along the longitudinal axis of MWCNTs.[18] In contrast, there is no nanoparticle on the MWCNT surface when glucose is absent in the hydrothermal synthesis (Figure S3, Supporting Information). Chang et al.[19] have reported that the composite of MoS_2 nanosheets and amorphous carbon can be synthesized using the glucose-assisted hydrothermal method and confirmed that MoS_2 nanosheets are uniformly dispersed in the carbonaceous material produced in situ by the hydrothermal carbonization of glucose. The scenario observed by Chang et al. could also be applied to our composite synthesis. As indicated by a red arrow in Figure 1c, the amorphous carbon produced by the hydrothermal carbonization of glucose is intercalated between the small-sized nanoparticles. In other words, the amorphous carbon serves as a binder for the assembly of nanoparticles. The EDS analysis of the composite sample (Figure 1d) reveals the presence of C, O, Si, Ni, and S elements, and the atomic ratio of Ni to S is estimated to be 3.0:2.0. To further characterize the identity and structure of the composite sample, XRD measurement was carried out. As shown in Figure 1e, all the identified peaks except the (002) reflection of MWCNTs can be attributed to the Ni_3S_2 phase (JCPDS card No. 30-0863). Furthermore, the averaged grain size of Ni_3S_2 nanoparticles is estimated using the Scherrer equation: $D = 0.89\lambda/(\beta \cos\theta)$, where λ is the employed X-ray wavelength, θ is the diffraction angle of the most intense diffraction peak ((110) reflection of Ni_3S_2), and β is the full width at half-maximum (fwhm) of the most intense diffraction peak.[20] The averaged grain size of the Ni_3S_2 nanoparticles (11.5 nm) is much smaller than that of the nanoparticles observed by TEM (42.5 nm). As a result, it is further confirmed that the Ni_3S_2 nanoparticles self-assemble into the large-sized nanoparticles with irregular shapes.

The electrochemical behavior of Ni_3S_2/MWCNT-NC was investigated using CV in a 2 M KOH solution. As shown in Figure 2a, the CV curve of Ni_3S_2/MWCNT-NC exhibits a pair of redox peaks in the potential range from 0 to 0.6 V. According to the previous studies of the electrochemical properties of nickel sulfide in a KOH solution, the redox peaks at around 0.4

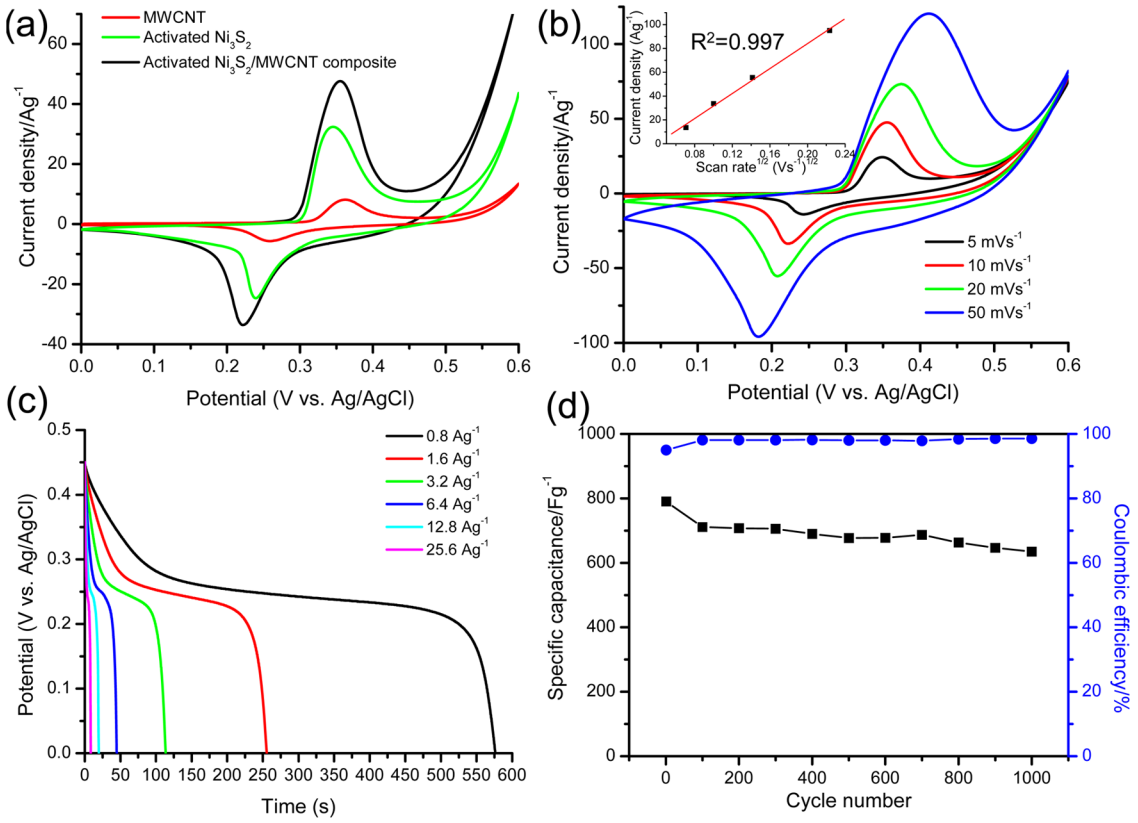

Figure 3. (a) CV curves of the MWCNT, the activated Ni_3S_2, and the activated Ni_3S_2/MWCNT-NC electrodes measured at a scan rate of 10 mV/s in 2 M KOH. (b) CV curves of the activated composite electrode recorded at different scan rates in 2 M KOH. The inset in part b shows the variation of the current density of the cathodic peak as a function of the square root of scan rate. (c) Discharge curves of the composite electrode at different current densities in 2 M KOH electrolyte. (d) The variations in specific capacitance and Coulombic efficiency of the activated composite electrode as a function of cyclic number at a current density of 3.2 A/g.

and 0.22 V can be attributed to the reversible redox reactions of Ni(II) ↔ Ni(III) as shown below.[13,14,21]

$$Ni_3S_2 + 3OH^- \leftrightarrow Ni_3S_2(OH)_3 + 3e^- \quad (1)$$

Interestingly, it is found that the area under the CV curve becomes large when the number of CV scans increases. The C_m value of the composite electrode can be estimated by integrating the area under the reduction peak of a stable CV and then dividing by the scan rate (v), the mass of the active material (m) in the electrode, and the potential window ($V_a - V_c$) according to the following equation.

$$C = \frac{1}{mv(V_a - V_c)} \int_{V_a}^{V_c} I(V)\, dV \quad (2)$$

At a high scan rate of 50 mV/s, the C_m value of the composite electrode is changed from 496 to 665 F/g after the consecutive CV scans. As a result, the increasing percentage of the C_m value for the composite electrode after the CV experiment is ca. 34%. To understand the origin of the capacitive enhancement of Ni_3S_2/MWCNT-NC, Ni_3S_2/MWCNT-NC after the CV experiment was characterized by TEM. As shown in Figure 2b, the morphology of the composite is changed significantly after the CV experiment. It seems that the irregularly shaped Ni_3S_2 nanoparticles disassemble into smaller components without the change of their composition (Figure S4, Supporting Information) in a KOH solution. For the composite electrode after CV experiment, the enhancement of its capacitive performance may be attributed to the fact that the small sizes of Ni_3S_2 nanoparticles make nearly full utilization of the electrode materials.[22,23] As a result, the consecutive CV scan in a KOH solution can be considered as the activation process for Ni_3S_2/MWCNT-NC. It is known that sodium hydroxide can serve as an efficient agent to remove the carbonaceous material on the surface of carbon nanotubes.[24] Therefore, it is assumed that the disassembly of irregular Ni_3S_2 nanoparticles may be attributed to the partial removal of carbonaceous material formed between small-sized Ni_3S_2 nanoparticles by KOH solution. However, the actual reasons for morphological change of the composite, requiring intense research efforts, are currently under investigation in our group.

Figure 3a shows the CV curves of the electrodes of MWCNTs, Ni_3S_2 powders, and Ni_3S_2/MWCNT-NC measured at a scan rate of 10 mV/s in 2 M KOH. In the CV plot of the MWCNT electrode, a pair of redox peaks probably ascribes to the redox reaction of electrolyte ions with the residual functional groups and structural defects in MWCNTs.[25] Compared with the MWCNT electrode, the Ni_3S_2 electrode after the activation process shows a larger area under the CV curve and thus possesses the superior capacitive property. On the basis of the areas under the CV curves, the C_m values of the MWCNT and the activated Ni_3S_2 electrodes are estimated to be 137 and 603 F/g, respectively. It is noteworthy that the electrode of Ni_3S_2/MWCNT-NC after activation treatment has the largest C_m value (866 F/g) among all the supercapacitor electrodes. Figure 3b shows the CV curves of the activated Ni_3S_2/MWCNT-NC electrode at the different scan rates. The C_m value is calculated to be 866 F/g at a scan rate of 10 mV/s.

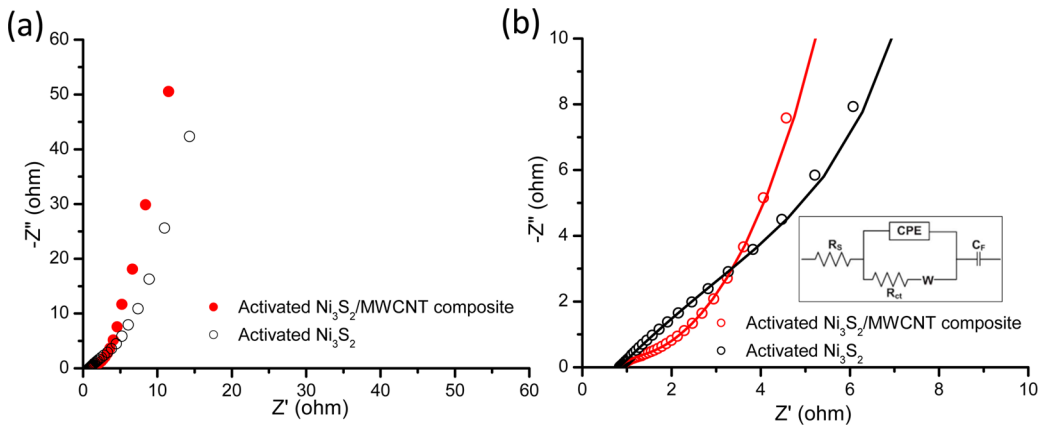

Figure 4. (a) Nyquist plots of the activated Ni_3S_2 and the activated Ni_3S_2/MWCNT-NC electrodes. (b) The enlarged Nyquist plots in the high frequency region. The black and red curves represent the data of EIS curve fitting for the activated Ni_3S_2 and composite electrodes, respectively. The inset shows the equivalent circuit used to simulate the Nyquist plots. In the equivalent circuit, R_s is the bulk solution resistance, R_{ct} is the Faradaic interfacial charge−transfer resistance, CPE represents the constant phase element accounting for a double-layer capacitance, Z_W is the Warburg impedance, and C_F is the Faradaic pseudocapacitor.

At a high scan rate of 50 mV/s, ca. 82% capacitance retention is observed, suggesting that the composite electrode shows a reasonable rate capability. The inset of Figure 3b shows that the cathodic peak currents increase linearly with the square root of the scan rate, indicating that the redox reactions of the Ni_3S_2 nanoparticles are rapid. According to the slopes shown in the insets of Figure 3b and Figure S5 (Supporting Information), the diffusion coefficient of electrolyte ions for the activated Ni_3S_2/MWCNT-NC electrode is 1.5 times higher than that of the activated Ni_3S_2 electrode, suggesting that the former has the better ion diffusion.

In Figure 3c, the galvanostatic charge/discharge curves of the activated Ni_3S_2/MWCNT-NC electrode obtained at different current densities exhibit a nonlinear profile as expected for the pseudocapacitive electrode. The C_m value can be estimated from the discharge section according to eq 1:

$$C_m = \frac{I \times \Delta t}{m \times \Delta V} \tag{3}$$

where I, Δt, ΔV, and m represent discharge current, discharge time, potential window, and the mass of the composite in the electrode, respectively. The C_m values of the activated Ni_3S_2/MWCNT-NC electrode are calculated to be 1024, 908, 806, 637, 560, and 480 F/g at 0.8, 1.6, 3.2, 6.4, 12.8, and 25.6 A/g, respectively. The aforementioned C_m values obtained at different current densities further verify that the rate capability of the activated Ni_3S_2/MWCNT-NC electrode is excellent, which is consistent with the result obtained from CVs. It is noteworthy that the C_m value of the activated Ni_3S_2/MWCNT-NC electrode is comparable to or even higher than the electrodes constructed by NiS nanoflakes (664 F/g at 4 A/g),[13] NiS hollow spheres (927 F/g at 4.08 A/g),[14] NiS nanoparticles (893 F/g at 5 A/g),[15] and Ni_3S_2/CNT composite (514 F/g at 4 A/g).[16] To get more information about the electrochemical stability of the composite electrode, consecutive charge−discharge cycles were performed at a current density of 3.2 A/g. As shown in Figure 3d, only an ∼20% decrease in a C_m value is observed after 1000 charge and discharge cycles, suggesting the great electrochemical stability of the activated Ni_3S_2/MWCNT-NC electrode. Furthermore, the composite electrode exhibits nearly 100% Coulombic efficiency over the entire cycling test.

To further understand the mechanism behind the excellent capacitive performance of the activated Ni_3S_2/MWCNT-NC electrode, EIS measurements were performed at a frequency range from 100 kHz to 0.01 Hz. As shown in Figure 4a, each Nyquist plot consists of a semicircle in the high frequency region and a straight line in the low frequency region. The charge transfer resistance (R_{ct}) corresponding to the diameter of a semicircle in the high frequency region can be evaluated by fitting the EIS spectra based on the equivalent circuit proposed in the inset of Figure 4b.[13] The R_{ct} value of the activated Ni_3S_2/MWCNT-NC electrode (0.7 Ω) is much smaller than that of the activated Ni_3S_2 electrode (8.99 Ω). The activated Ni_3S_2/MWCNT-NC electrode shows faster reaction kinetics than the activated Ni_3S_2 electrode due to the fact that the conductive MWCNT network facilitates rapid electron transfer between the active materials and the charge collector. As shown in the low frequency regions of EIS spectra, the activated Ni_3S_2/MWCNT-NC electrode has the more vertical straight line than the activated Ni_3S_2 electrode, which suggests that the former shows the better ion diffusion. Compared with the activated Ni_3S_2 electrode, the activated Ni_3S_2/MWCNT-NC has an interconnected porous MWCNT network and uniform distribution of Ni_3S_2 nanoparticles on it, which enables electrolyte ions to diffuse easily. The aforementioned EIS studies verify that the synergistic effect of the Ni_3S_2 nanoparticles and the conductive MWCNTs is responsible for the enhancement of capacitive performance of the activated Ni_3S_2/MWCNT-NC electrode.

To evaluate the capacitive performance of the Ni_3S_2/MWCNT-NC electrode in a full-cell configuration, an asymmetric supercapacitor device was fabricated by using the activated Ni_3S_2/MWCNT-NC as the cathode and AC as the anode (denoted as Ni_3S_2/MWCNT-NC//AC). As shown in Figure S6a (Supporting Information), the CV curves of the AC electrode collected at different scan rates in a 2 M KOH solution exhibit nearly rectangular shapes, suggesting that the AC electrode has excellent electrochemical double layer capacitance. Furthermore, the galvanostatic charge/discharge curves of the AC electrode measured at different current densities are symmetric and linear, which clearly manifests the double layer capacitive behavior of the AC electrode (Figure S6b, Supporting Information). The C_m values of the AC

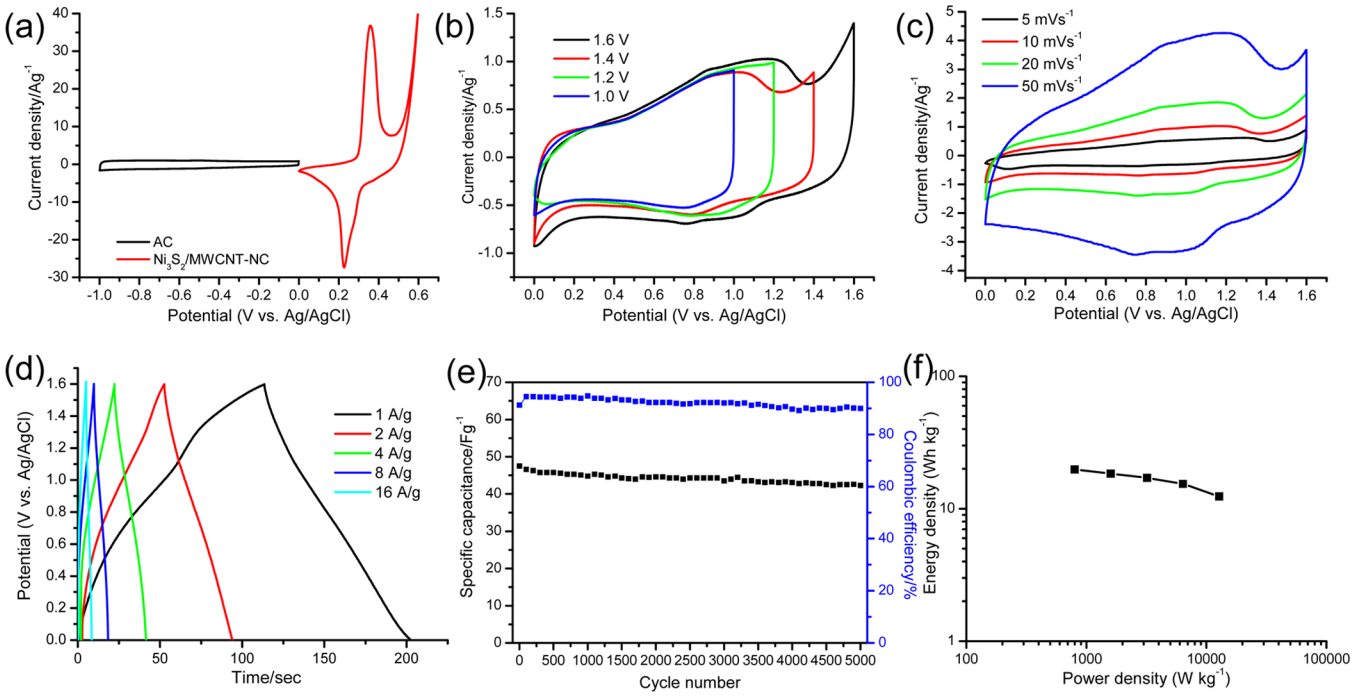

Figure 5. (a) CV curves of Ni_3S_2/MWCNT-NC and AC electrodes measured at a scan rate of 10 mV/s in a three-electrode system. CV curves of the Ni_3S_2/MWCNT-NC//AC device collected at (b) the different voltages at a scan rate of 10 mV/s and (c) the different scan rates in the potential window of 0−1.6 V. (d) Galvanostatic charge/discharge curves of the Ni_3S_2/MWCNT-NC//AC device recorded at different current densities. (e) The variations in specific capacitance and Coulombic efficiency of the Ni_3S_2/MWCNT-NC//AC device as a function of cyclic number at a current density of 4 A/g. (f) Ragone plot of the Ni_3S_2/MWCNT-NC//AC device.

electrode are calculated to be 94.8, 88.8, 83.6, and 78.4 F/g at 1, 2, 4, and 8 A/g, respectively. To obtain a good electrochemical performance for an asymmetric supercapacitor, the charge balance between the cathode and the anode should be satisfied. Therefore, on the basis of the C_m values and potential windows of two electrodes, the optimum loading mass ratio of Ni_3S_2/MWCNT-NC to AC is estimated to be 0.21.

In Figure 5a, the cell voltage can be expressed as the sum of the potential ranges of Ni_3S_2/MWCNT-NC cathode and AC anode, which shows that the potential window is between 0.6 and −1.0 V vs Ag/AgCl. Therefore, the Ni_3S_2/MWCNT-NC//AC device could achieve a maximum working voltage of 1.6 V. In Figure 5b, the CV curves of a Ni_3S_2/MWCNT-NC//AC device measured at different working voltages at a scan rate of 10 mV/s exhibit a stable potential window up to 1.6 V. Furthermore, the distorted rectangular CV curves may be attributed to the contribution from the pseudocapacitive cathode (Figure 5c). The galvanostatic charge/discharge curves of the asymmetric supercapacitor were measured at the current densities from 1 to 16 A/g in a potential window of 0−1.6 V. As shown in Figure 5d, the Ni_3S_2/MWCNT-NC//AC device demonstrates a good capacitive behavior based on its symmetric and linear charge/discharge curves. Furthermore, the C_m values of the Ni_3S_2/MWCNT-NC//AC device are calculated to be 55.8, 52.0, 48.0, 43.5, and 35.0 F/g at 1, 2, 4, 8, and 16 A/g, respectively. To test the electrochemical stability of the asymmetric supercapacitor, consecutive charge−discharge cycles were performed at a current density of 4 A/g. As shown in Figure 5e, only 10% decrease in a C_m value is observed after 5000 charge/discharge cycles. Furthermore, the Coulombic efficiency of the Ni_3S_2/MWCNT-NC//AC device remains as high as 90% after 5000 charge/discharge cycles. This excellent electrochemical stability suggests a highly reversible Faradaic reaction between the electrolyte and the Ni_3S_2/MWCNT-NC.[26] In Figure 5f, the Ragone plot related to power densities (P) and energy densities (E) is further used to evaluate the performance of the Ni_3S_2/MWCNT-NC//AC device. The energy density and power density of the asymmetric supercapacitor were calculated by the following equations:

$$E = 1/2 \times C_m \times (\Delta V)^2 \quad (4)$$

$$P = E/\Delta t \quad (5)$$

where C_m is the specific capacitance calculated on the basis of the mass loading of active materials on both electrodes, ΔV is the operating voltage of the cell, and Δt is the discharge time. The Ni_3S_2/MWCNT-NC//AC device can deliver a high energy density of 19.8 Wh/kg at a power density of 798 W/kg and still maintain 15.4 Wh/kg at a high power density of 6.4 kW/kg. Given that the C_m value of the AC anode is not very high (95 F/g), the energy density of the asymmetric supercapacitor is expected to be further improved by replacing the AC electrode with other carbonaceous electrodes with the high C_m values. It is noteworthy that the Ni_3S_2/MWCNT-NC//AC device exhibits a superior energy density at a high power density compared with previously reported asymmetric supercapacitors including NiW-70//AC (15.1 Wh/kg at 4.8 kW/kg),[27] Ni_xCo_{1-x}LDH−ZTO//AC (9.7 Wh/kg at 5.82 kW/kg),[28] $NaMnO_2$//AC (13.2 Wh/kg at 1.0 kW/kg),[29] MnO_2 nanorods//AC (17 Wh/kg at 2.0 kW/kg),[30] $LiTi_2(PO_4)_3$//AC (15 Wh/kg at 1.0 kW/kg),[31] and $K_{0.27}MnO_2$ $0.6H_2O$//AC (17.6 Wh/kg at 2.0 kW/kg).[32] Finally, we assembled two asymmetric supercapacitors in series to demonstrate the practical applications of the Ni_3S_2/MWCNT-NC//AC device, and the device successfully lit a red light-emitting diode (LED) (driving voltage 1.8 V) after charging (Figure S7, Supporting

Information). Therefore, the aforementioned results suggest that the Ni_3S_2/MWCNT-NC//AC device with high energy density shows a great potential application as an inexpensive energy storage system.

4. CONCLUSIONS

We have successfully developed the glucose-assisted hydrothermal method to directly grow Ni_3S_2 nanoparticles on MWCNTs and demonstrated that this hierarchical hybrid can serve as the electrode material for supercapacitors. It is found that the use of glucose in hydrothermal reaction is essential to the formation of this hybrid structure. As evidenced by TEM observations, the Ni_3S_2 nanoparticles deposited on MWCNTs disassemble into the smaller components after the composite electrode is activated by the consecutive CV scan in a 2 M KOH solution. As a result, the active surface area of the Ni_3S_2 nanoparticles is increased, which further enhances the electrochemical performance of Ni_3S_2/MWCNT-NC. Furthermore, the systematic CV measurements verify that the activated Ni_3S_2/MWCNT-NC electrode shows the best capacitive performance compared with the activated Ni_3S_2 and MWCNTs electrodes. EIS measurements reveal that the activated Ni_3S_2/MWCNT-NC has a lower R_{ct} value and better ion diffusion than the activated Ni_3S_2 electrode. Due to the synergistic effect of the Ni_3S_2 nanoparticles and MWCNTs, the activated Ni_3S_2/MWCNT-NC electrode exhibits a high specific capacitance of 800 F/g and great cycling stability at a current density of 3.2 A/g. Furthermore, an asymmetric supercapacitor was assembled by using Ni_3S_2/MWCNT-NC as the cathode and AC as the anode, respectively. The Ni_3S_2/MWCNT-NC//AC device can be reversibly charged/discharged at a maximum cell voltage of 1.6 V and obtain a high specific capacitance of 55.8 F/g at 1 A/g, which delivers a maximum energy density of 19.8 Wh/kg at a power density of 798 W/kg. More importantly, the Ni_3S_2/MWCNT-NC//AC device preserves 90% of its initial capacitance and retains 90% Coulombic efficiency after 5000 charge/discharge cycles are performed at a current density of 4 A/g. Such excellent capacitive performance suggests that the Ni_3S_2/MWCNT-NC//AC device shows a great potential application as an inexpensive energy storage system.

■ ASSOCIATED CONTENT

Supporting Information

The high resolution TEM and SAED images of Ni_3S_2/MWCNT-NC, TEM image of the mixture of Ni_3S_2 particles and MWCNTs, XRD pattern of the activated Ni_3S_2/MWCNT-NC, CV curves of Ni_3S_2 and AC electrodes, and a demonstration of lightening up a red LED using Ni_3S_2/MWCNT-NC//AC devices. This material is available free of charge via the Internet at http://pubs.acs.org.

■ AUTHOR INFORMATION

Corresponding Author

*E-mail: twlin@thu.edu.tw. Phone/Fax: +886(4)23596233.

Notes

The authors declare no competing financial interest.

■ ACKNOWLEDGMENTS

This research was supported by the National Science Council Taiwan (NSC 101-2113-M-029-003).

■ REFERENCES

(1) Simon, P.; Gogotsi, Y. *Nat. Mater.* **2008**, *7*, 845−854.
(2) Hall, P. J.; Mirzaeian, M.; Fletcher, S. I.; Sillars, F. B.; Rennie, A. J. R.; Shitta-Bey, G. O.; Wilson, G.; Cruden, A.; Carter, R. *Energy Environ. Sci.* **2010**, *3*, 1238−1251.
(3) Wang, G. P.; Zhang, L.; Zhang, J. J. *Chem. Soc. Rev.* **2012**, *41*, 797−828.
(4) Kotz, R.; Carlen, M. *Electrochim. Acta* **2000**, *45*, 2483−2498.
(5) Hu, C. C.; Chang, K. H.; Lin, M. C.; Wu, Y. T. *Nano Lett.* **2006**, *6*, 2690−2695.
(6) Zhang, H.; Cao, G.; Wang, Z.; Yang, Y.; Shi, Z.; Gu, Z. *Nano Lett.* **2008**, *8*, 2664−2668.
(7) Dong, X. C.; Xu, H.; Wang, X. W.; Huang, Y. X.; Chan-Park, M. B.; Zhang, H.; Wang, L. H.; Huang, W.; Chen, P. *ACS Nano* **2012**, *6*, 3206−3213.
(8) Saravanakumar, B.; Purushothaman, K. K.; Muralidharan, G. *ACS Appl. Mater. Interfaces* **2012**, *4*, 4484−4490.
(9) Liang, L.; Liu, J.; Windisch, C. F.; Exarhos, J. G. J.; Lin, Y. *Angew. Chem., Int. Ed.* **2002**, *41*, 3665−3668.
(10) Parthasarathy, R. V.; Martin, C. R. *Chem. Mater.* **1994**, *6*, 1627−1632.
(11) Cao, Y.; Mallouk, T. E. *Chem. Mater.* **2008**, *20*, 5260−5265.
(12) Chang, H. H.; Chang, C. K.; Tsai, Y. C.; Liao, C. S. *Carbon* **2012**, *50*, 2331−2336.
(13) Chou, S. W.; Lin, J. Y. *J. Electrochem. Soc.* **2013**, *160*, D178−182.
(14) Zhu, B. T.; Wang, Z.; Ding, S.; Chen, J. S.; Lou, X. W. *RSC Adv.* **2011**, *1*, 397−400.
(15) Hou, L.; Yuan, C.; Li, D.; Yang, L.; Shen, L.; Zhang, F.; Zhang, X. *Electrochim. Acta* **2011**, *56*, 7454−7459.
(16) Zhu, T.; Wu, H. B.; Wang, Y.; Xu, R.; Lou, X. W. *Adv. Energy Mater.* **2012**, *2*, 1497−1502.
(17) Xing, Z.; Chu, Q.; Ren, X.; Tian, J.; Asiri, A. M.; Alamry, K. A.; Al-Youbi, A. O.; Sun, X. *Electrochem. Commun.* **2013**, *32*, 9−13.
(18) Ding, S. J.; Chen, J. S.; Lou, X. W. *Chem.—Eur. J.* **2011**, *17*, 13142−13145.
(19) Chang, K.; Chen, W.; Ma, L.; Li, H.; Li, H.; Huang, F.; Xu, Z.; Zhang, Q.; Lee, J. Y. *J. Mater. Chem.* **2011**, *21*, 6251−7.
(20) Patterson, A. L. *Phys. Rev.* **1939**, *56*, 978−982.
(21) Xing, Z.; Chu, Q.; Ren, X.; Ge, C.; Qusti, A. H.; Asiri, A. M.; Al-Youbi, A. O.; Sun, X. *J. Power Sources* **2014**, *245*, 463−467.
(22) Yan, J.; Sun, W.; Wei, T.; Zhang, Q.; Fan, Z.; Wei, F. *J. Mater. Chem.* **2012**, *22*, 11494−11502.
(23) Wang, D. W.; Li, F.; Liu, M.; Lu, G. Q. *Angew. Chem., Int. Ed.* **2008**, *47*, 373−376.
(24) Salzmann, C. G.; Llewellyn, S. A.; Tobias, G.; Ward, M. A. H.; Huh, Y.; Green, M. L. H. *Adv. Mater.* **2007**, *19*, 883−887.
(25) Chen, S.; Zhu, J.; Zhou, H.; Wang, X. *RSC Adv.* **2011**, *1*, 484−489.
(26) Lei, Z.; Zhang, J.; Zhao, X. S. *J. Mater. Chem.* **2012**, *22*, 153−160.
(27) Niu, L.; Li, Z.; Xu, Y.; Sun, J.; Hong, W.; Liu, X.; Wang, J.; Yang, S. *ACS Appl. Mater. Interfaces* **2013**, *5*, 8044−8052.
(28) Wang, Wu.; Sumboja, A.; Lin, M.; Yan, J.; Lee, P. S. *Nanoscale* **2012**, *4*, 7266−7272.
(29) Qu, Q. T.; Shi, Y.; Tian, S.; Chen, Y. H.; Wu, Y. P.; Holze, R. *J. Power Sources* **2009**, *194*, 1222−1225.
(30) Qu, Q.; Zhang, P.; Wang, B.; Chen, Y.; Tian, S.; Wu, Y.; Holze, R. *J. Phys. Chem. C* **2009**, *113*, 14020−14027.
(31) Luo, J. Y.; Xia, Y. Y. *J. Power Sources* **2009**, *186*, 224−227.
(32) Qu, Q. T.; Li, L.; Tian, S.; Guo, W. L.; Wu, Y. P.; Holze, R. *J. Power Sources* **2010**, *195*, 2789−2794.